Algorithm for the determination of intrinsic optical constants of metal films: application to aluminum

Aleksandar D. Rakić

Optical and electron-energy-loss data for evaporated-aluminum films have been critically analyzed and used in an iterative, self-consistent algorithm that represents a combination of the Kramers–Kronig analysis and the semiquantum-model application. The novel values of the intrinsic optical functions of aluminum have been determined in a wide spectral range from 200 μm (6.2 meV) to 0.12 nm (10 keV). These functions are in accordance with recent calculations by Lee and Chang [Phys. Rev. B **49,** 2362 (1994)], with dc conductivity measurements, and are in good agreement with both peak positions and line widths obtained from electron-energy-loss experiments. The results are examined for internal consistency by inertial and *f*-sum rules.

Key words: Kramers-Kronig analysis, optical constants, aluminum, metal-film optics.

1. Introduction

The purpose of this paper is to present an efficient and accurate algorithm for the analysis of optical data in a wide spectral range. An iterative, self-consistent method combining the model application and the Kramers–Kronig inversion of reflectivity and extinction coefficient is employed to determine the values of the optical functions of aluminum from 200 μm (6.2 meV) to 0.12 nm (10 keV). Although there has been considerable theoretical[1–8] and experimental[9–22] interest in the optical properties of aluminum films, including several excellent papers[23–27] dealing with the problem of the construction of a self-consistent set of optical functions of aluminum over a wide spectral range, the values of the optical functions of Al in some spectral regions need to be reconsidered.

The latest significant analysis of the experimental data was performed by Shiles *et al.*[26] in the early 1980's. Their analysis indicated an excess oscillator strength in the soft x-ray region in the vicinity of the *L* edge that possibly was caused by layers of surface oxide on the specimens used for transmission measurements. Optical constants derived by Shiles *et al.*[26] satisfy all the major optical-sum rules and are believed to be the most accurate composite published hitherto.

Since then several measurements[28–34] have been published, some of them in regions for which no optical measurements had existed before, which has widened the spectral range in which analysis could be performed and also provided the opportunity to reanalyze the existing data in another way. However, in the light of these measurements and of new theoretical results, a few improvements of the analysis reported in Ref. 26 could be performed.

First one refers to reflectivity in the visible and ultraviolet (UV) ranges. In the values for reflectivity $R(\omega)$ obtained by Shiles *et al.*,[26] $R(\omega)$ is observed to increase between 4 and 11 eV. All relevant measurements show a decrease instead of an increase of $R(\omega)$ in that range. Moreover, secondary structure in the reflectance spectrum[9,14–16] between 1.5 and 3 eV in Ref. 26 is removed in Ref. 26 by interpolation with a smooth rising function. According to measurements by Jiles and Staines[35] of the piezoreflectance spectrum of Al between 1.25 and 5.2 eV and band structure calculations by Singhal and Callaway,[4] Nelson and Bunyan,[5] and Szmulowicz and Segall[6] that stress the significance of the W-point transition ($W_3 \rightarrow W_1$) at 2.1 eV, it is evident that the structure observed around 2.1 eV in Ref. 9 is not spurious. Results of Jiles and Staines[35] suggest the importance of the two transitions along the Δ and Σ directions, which may contribute to the structure at approxi-

The author is with the Faculty of Electrical Engineering, University of Belgrade, Bulevar Revolucije 73, P.O. Box 816, 11000 Belgrade, Yugoslavia.

Received 13 September 1994; revised manuscript received 9 December 1994.

0003-6935/95/224755-13$06.00/0.

mately 4.5–4.6 eV. Calculations by Szmulowicz and Segall[6] and recent work by Lee and Chang[8] also show the structure in a joint density of states at approximately 6.7 eV; it results from transitions at point X ($X_1 \rightarrow X_5'$), which they expect to be of minor significance to the optical spectrum.

The second problem is related to data in the far infrared. Values used by Shiles *et al.*[26] end at 0.04 eV. The lowest pronounced interband transition for Al occurs at 0.4 eV. For Al as a metal that possesses several small band gaps (a few tens of milli-electron volts), it is apparent that the interband absorption in the far-infrared part of the spectrum is usually attributed to Drude absorption,[3,6] which leads to overestimations of the value of the damping frequency of the intraband (Drude) part. It is suggested by Lee and Chang[8] that the onset frequency of the interband transitions is 100 meV, whereas some earlier studies[6] claim that there is no onset frequency as $\omega \rightarrow 0$. This makes the extrapolation to zero by means of the Drude model uncertain. In this paper, measurements by Ordal *et al.*[29] and an efficient method for the reduction of the uncertainties in the Drude-model parameters proposed by Smith and Segal[36] are used to perform a reliable extrapolation to the zero frequency.

The paper is organized as follows: In Section 2 the review and interpretation of experimental data are given. In Section 3.A the procedure used to fit the semiquantum model is described. Section 3.B outlines the Kramers–Kronig (KK) inversion procedure. In Section 4 the results obtained are compared with earlier results and examined by means of the optical sum rules. Conclusions are presented in Section 5.

2. Experimental Data

The initial set of data used in this paper was carefully selected from the large amount of published reflectance–transmittance and ellipsometric measurements. We have focused on the meaurements performed with Al films of controlled (or known) roughness that were prepared in ultrahigh vacuum (10^{-10} Torr) or in conventional vacuum with high evaporation rates. Between 6.2 meV (200 μm) and 24.8 eV the following data were used:

- 6.2–37.8 meV, from Ordal *et al.*,[29]
- 44.3 meV–2.25 eV, from Bennett *et al.*,[9]
- 2.27–3.44 eV, from Hass and Waylonis,[10]
- 4.00–11.72 eV, from Endriz and Spicer,[11]
- 15.0–16.0 eV, from Ditchburn and Freeman,[12] and
- 16.53–24.80 eV, from Hunter.[13]

Several important differences exist between this interpretation of the reflectance spectrum and those of the previous analyses.[23,24,26,37] The experimental spectrum is widened far in the extreme infrared with the measurements by Ordal *et al.*[29] between 6.2 and 37.8 meV. These nonresonant-cavity transmission measurements provided trial reflectance values in the region where, because of the extremely high reflectance of Al, no direct reflectance or absorptance measurements exist. The data from Bennett *et al.*[9] suggest that a secondary shoulder exists between 1.5 and 3 eV (see Fig. 1) and that it is superimposed on the reflectance dip associated with band-to-band transitions near 1.5 eV. Measurements by Hass and Waylonis,[10] Schulz,[14] Schulz and Tangherlini,[15] and Beaglehole[16] also show a structure superimposed on the main reflectance dip, whereas those of Mathewson and Myers[17] do not. Assuming that there was no secondary structure, Shiles *et al.*[26] employed the smooth interpolation between 1.66 and 3.0 eV and surpassed the highest experimental values by 0.6%; they were considerably above the quoted experimental error (0.1%)[9] in that part of the spectrum. The calculated joint density of states by Szmulowicz and Segall[6] and Lee and Chang[8] also show the structure at 2.1 eV that is due to the onset of transitions in the vicinity of point W (i.e., $W_3 \rightarrow W_1$). Piezoreflectance studies by Jiles and Staines[35] present a more definitive argument of the existence of the secondary structure in the vicinity of 2.1 eV. Reflectance calculated from the optical constants from ellipsometric measurements by Bodo and Gergely[31] from 2.2 to 3.1 eV are in excellent agreement with the reflectance measurement employed in this study. They have also shown[31] that their values of intrinsic optical constants can be obtained after correction for surface-oxide-layer absorption from the previously published results of Blanco *et al.*[28] and Hass and Waylonis.[10] Hence, in the region from 2.27 to 3.44 eV, we have chosen the data from Hass and Waylonis[10] that has the highest reflectance values in that range, which are usually connected with superior sample surfaces. The smooth-surface-sample reflectance data from Endriz and Spicer[11] that were employed between 4 and 11.72 eV show the decrease of reflectance with frequency. In contrast, the $R(\omega)$ data obtained by Shiles *et al.*[26] increase with frequency and show discrepancies from the experimental values up to

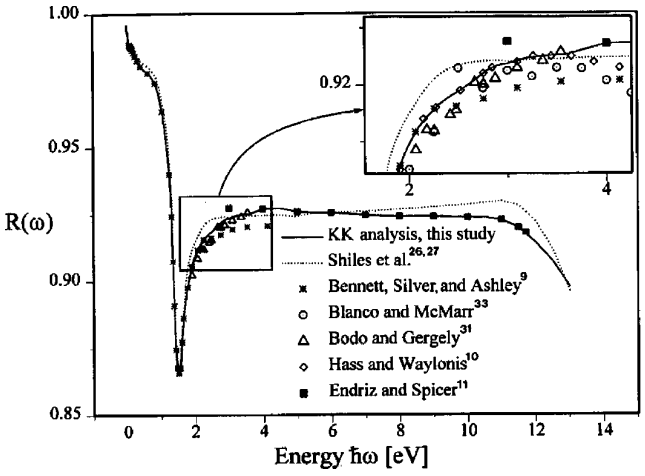

Fig. 1. Comparison of the measured Al reflectance to $R(\omega)$ obtained with the self-consistent KK analysis plus selected experimental data.

0.8% at the borders of the aforementioned region, which considerably exceeds the experimental uncertainty. Values of $R(\omega)$ obtained in the present study are in close agreement with relevant experimental data.

In the vicinity of the volume plasmon, the reflectance of Al drops abruptly from almost 92% to 1%, so it is important to determine the slope of the reflectance curve accurately. In this region, data from Hunter[13] and from Ditchburn and Freeman[12] are relevant. Recent measurements by Windt *et al.*[30] stress the agreement in slope with those of Ditchburn and Freeman,[12] but with lower reflectance values that are probably due to the considerable sample roughness ($\sigma = 2.13$ nm $\pm$ 0.3 nm). Although the authors claim their values have been corrected for surface-roughness effects by including the Debye–Waller factor in Fresnel equations, it is evident that the reflectance calculated from their optical constants is in good agreement with directly measured values of $R(\omega)$ for a rough-surface sample by Endriz and Spicer[11] that had a rms surface roughness $\sigma = 2.7$ nm.

Above 25 eV, reflectance measurements are sparse and unreliable. In that part of the spectrum the extinction coefficient k is usually determined from absorption measurements. Values of $k(\omega)$ from the analysis of Shiles *et al.*[26] (tabulated in Ref. 27) were used between ω_p and 10 keV as trial values. These values closely agree with measurements by Balzarotti *et al.*[18] in the vicinity of the L edge. Data from Balzarotti *et al.*[18] have the same structure as those from Gahwiller and Brown[19] and Haensel *et al.*,[20] but with significantly lower values of $k(\omega)$ (from 11% to 14%). This probably inspired the so successfully performed ad hoc reduction of $k(\omega)$ values above the L-shell absorption edge by Shiles *et al.*[26] Novel values of $k(\omega)$ published by Windt *et al.*[30] have still lower values in the region of overlap (72–500 eV), which indicates that the set obtained by Shiles *et al.*[26] is still the best currently available composition above the plasma frequency.

3. Numerical Procedure

It is well known that for the KK analysis it is necessary to know one of the optical functions in the entire spectrum. However, no optical function can be measured directly in all regions from x-rays to microwaves. Combining the results from a number of sources it is possible to estimate values of the chosen optical function over a wide spectral range. There are some wavelength regions in which optical measurements are not feasible, and it is necessary to make extrapolations of the behavior of the optical functions in those regions. Extrapolations are usually the weakest points of the KK-analysis procedure.

If the extinction coefficient $k(\omega)$ is chosen as a starting function, a combination of the model and ellipsometric data should be employed to estimate $k(\omega)$ values in the IR and UV. If the reflectivity $R(\omega)$ is chosen, extrapolation of the $R(\omega)$ behavior from plasma frequency ω_p to infinity should be performed. This is connected with problems of loss of the structure in the vicinity of the L and K edges and usually poor agreement with experimental results. It is evident that, in one cycle of the KK inversion, good results cannot be obtained.

In this paper I discuss a self-consistent KK procedure combining the $k(\omega)$ inversion, $R(\omega)$ inversion, and semiquantum-model (oscillator-model) application in an iterative algorithm for generation of a self-consistent set of optical functions over the entire spectral range.

A. Model Used for Generation of the Initial Data

If the extinction coefficient is chosen as a starting function it is necessary to use a specific model to calculate trial values of $k(\omega)$ in the region for which no measurements exist. The first approximation for $k(\omega)$ is provided by the semiquantum model from $\omega_l = 6.2$ meV to ω_p; experimental values are employed from ω_p to $\omega_h = 10$ keV, and asymptotic expansion from ω_h to infinity. I briefly discuss the applied model, which was usually employed to obtain the final values for the optical constants and dielectric function of metals.[37,38] It was shown[3,23,39,40] that $\epsilon_r(\omega)$ could be expressed in the form that separates explicitly the intraband effects (usually referred to as free-electron effects) from interband effects (usually associated with bound electrons). In the present study the following model is used:

$$\hat{\epsilon}_r(\omega) = \hat{\epsilon}_r^{(f)}(\omega) + \hat{\epsilon}_r^{(b)}(\omega). \tag{1}$$

The intraband part $\hat{\epsilon}_r^{(f)}(\omega)$ of the dielectric constant is a well-known free-electron model,[41] possibly containing the frequency-dependent parameter[42–44] Γ_0:

$$\hat{\epsilon}_r^{(f)}(\omega) = 1 - \frac{{\Omega_p}^2}{\omega(\omega + i\Gamma_0)}. \tag{2}$$

The interband part of the dielectric constant $\hat{\epsilon}_r^{(b)}(\omega)$ is a simple semiquantum model resembling the Lorentz result for insulators:

$$\hat{\epsilon}_r^{(b)}(\omega) = -\sum_{j=1}^{k} \frac{f_j {\omega_p}^2}{(\omega^2 - {\omega_j}^2) + i\omega\Gamma_j}, \tag{3}$$

where ω_p is the plasma frequency and k is the number of interband transitions with frequency ω_j, oscillator strength f_j, and lifetime $1/\Gamma_j$. Also $\Omega_p = \sqrt{f_0}\omega_p$ is the plasma frequency associated with intraband transitions, f_0 is the oscillator strength for electrons contributing in intraband processes, and $\Gamma_0 = \Gamma_0' + \omega^2\tau$ is the intraband-damping constant. It should be mentioned that Ω_p, given by

$$\Omega_p = \left(\frac{N_{\mathrm{eff},fe} e^2}{m\epsilon_0}\right)^{1/2}, \tag{4}$$

is not the frequency of the volume plasmon $[\epsilon_r(\Omega_p) \neq 0]$ and that the electron number density $N_{\mathrm{eff},fe}$ in Eq. (4) is not the valence-band electron concentration.

They are only parameters that describe the behavior of the intraband part of the conduction-electron spectrum. However, the distinction between the intraband plasma frequency Ω_p and the volume plasmon frequency ω_p should be emphasized. Plasma frequency ω_p (volume plasmon) is determined as a zero of the real part of the dielectric constant $[\epsilon_{r1}(\omega_p) = 0]$. Whereas the volume plasmon includes intraband and interband processes, the intraband plasma frequency Ω_p is connected with the effective number density of conduction electrons contributing to the intraband processes and represents the zero of the free-electron part of the dielectric constant, *viz.* $\epsilon_{r1}{}^{(f)}(\Omega_p) = 0$.

As has been mentioned above, the plasma frequency ω_p can be determined as a zero of the $\epsilon_{r1}(\omega)$ or from the crossing of the $n(\omega)$ and $k(\omega)$; $(\epsilon_{r1} = n^2 - k^2)$. It is possible to determine the plasma frequency from the position of the pole in the electron-energy-loss function[45] $\mathrm{Im}[-1/\hat{\epsilon}_r(\omega)]$, which has a sharp maximum corresponding to the excitation of the volume plasmon. These oscillations occur at ω_p, the conduction-electron plasma frequency. The plasma frequency corresponding to a number density of 3 electrons/Al atom (used by Powell[37]) is $\omega_p = 15.78$ eV. The plasma frequency estimated from the critical wavelength, which marks the transition from optically reflecting to optically transparent behavior, is $\lambda_c = 83.7$ nm, $[\omega_p = 14.8(0)$ eV], according to Ref. 13; $\lambda_c = 84.0$ nm, $[\omega_p = 14.7(6)$ eV], according to Ref. 21; $\lambda_c = 82.6$ nm, $[\omega_p = 15.0(0)$ eV], according to Ref. 12. Estimations performed on the basis of electron-energy-loss measurements also give a value close to 15 eV: $\omega_p = 15.2$ eV (Ref. 23), $\omega_p = 15.3$ eV (Ref. 3), and $\omega_p = 15.0(5)$ eV (Ref. 26), the last value's being obtained from a number of recent measurements discussed in (Ref. 26). Recent calculations of the plasma frequency with the exchange-correlation corrections of Lee and Chang[8] provide the value $\omega_p = 15.28$ eV, with a further reduction of 0.35 for the core polarization effect yielding $\omega_p = 14.93$ eV. The value of ω_p that is employed in this study and is consistent with the electron-energy-loss-function peak position (which was calculated from our values of the dielectric constant obtained from the KK inversion) is $\omega_p = 14.94$ eV. This value is used in the oscillator model. The electron-energy-loss function calculated from the dielectric constant obtained with the KK procedure in this work is presented in Fig. 2, with the full width at half-maximum $\Delta E_{1/2} = 0.48$ eV value's being in accordance with the experimental value[26] of $\Delta E_{1/2} \approx 0.5$ eV. To fit the oscillator model to the reflectance data I found that it proved useful to obtain the initial values of the Drude-model parameters Ω_p (i.e., $f_0 = \Omega_p{}^2/\omega_p{}^2$) and Γ_0 by fitting the Drude model to reflectance data in the wavelength region dominated by intraband absorption before proceeding further with a multiparameter fit. Parameters that were determined in such a manner inevitably contain the part of the oscillator strength that should be attributed to the interband spectrum if the fitting is performed for relatively high frequencies, or they are unreliable if the fitting is constrained to the extreme infrared, but at this stage of the procedure this effect is not critical. Initial values for the oscillator frequencies in (3) were obtained from the band structure of aluminum.[3,4,6,8,35] Interband transitions interpreted with oscillators in a semiquantum model are located at approximately 0.40, 1.56, 2.10, and 4.50 eV.

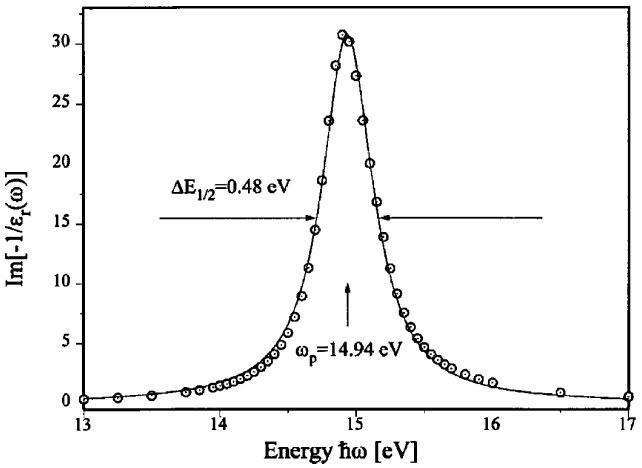

Fig. 2. Electon-energy-loss function calculated from values of the dielectric function determined with the KK analysis in this paper (denoted by the circled dots). The solid line represents the data from the Lorentz function with the center position at $\omega_p = 14.94$ eV and the full width at half-maximum $\Delta E_{1/2} = 0.48$ eV.

Thus the semiquantum-model parameters are determined through the performance of the multiparameter least-squares fit to the experimental reflectance data. The fitting routine is based on a modified Levenberg–Marquardt algorithm. The final values of the parameters are presented in Table 1. The oscillator strengths are based on a conduction-electron plasma frequency of $\omega_p = 14.94$ eV.

The discrepancies between the calculated and the experimental values of $R(\omega)$ lie within the borders of experimental uncertainties in a wide range from $\omega_l = 6.2$ meV to 25 eV. To my knowledge this is the parameterization of the optical constants of Al that is in good agreement with the experiment in a much wider spectral range than those published hitherto.

With this choice of parameters the model adequately describes not only the well-known 0.4- and 1.5-eV transitions, but also the 2.11- and 4.59-eV transitions. Moreover, the spurious intraband transition at 11.6 eV that was introduced by Powell,[37]

Table 1. Semiquantum-Model (Oscillator-Model) Parameter Values Employed for the Calculation of Trial Values of $k(\omega)$ between $\omega_l = 6.2$ meV and $\omega_p = 14.94$ eV

j	f_j	Γ_j (eV)	ω_j (eV)
0	0.632	0.075	0
1	0.109	0.44	0.34
2	0.096	0.45	1.57
3	0.122	1.41	2.11
4	0.024	2.82	4.59

which should be attributed to surface plasmon coupling and which cannot be observed from the experimental data used in this paper, is omitted. The interband transition at 0.4 eV was not separated from the intraband term by Powell.[37] His intraband component includes an amount of interband oscillator strength that leads to a large overestimate of the intraband-damping constant Γ_0 and the corresponding electron number density; as a consequence, the dc conductivity σ_0 was underestimated. As a result of this, large discrepancies between the experimental and the calculated values for the dielectric constant, the refractive index, and the extinction coefficient occurs, especially in the far-infrared region.

The model was employed merely to generate the initial reflectance values in the region between 11.7 and 15 eV, where optical measurements are not reliable, and in the first stage of the KK procedure to provide the first trial values for the extinction coefficient from $\omega_l = 6.2$ meV to $\omega_p = 14.94$ eV. The calculated values for $k(\omega)$ are in good agreement with the ellipsometric measurements by Mathewson and Myers,[17] the intrinsic optical constants from Bodo and Gergely,[31] and recent measurements by Nguyen *et al.*[34] in the region of overlap.

B. KK Inversion of $k(\omega)$ and $R(\omega)$

The extinction coefficient is used as a starting function in the iterative KK procedure. The semiquantum model provides values between $\omega_l = 6.2$ meV and $\omega_p = 14.94$ eV. From ω_p to $\omega_h = 10$ keV, the data from Shiles *et al.*[26,27] were employed. The dispersion relation connecting the refractive index $n(\omega)$ and the extinction coefficient $k(\omega)$ in its usual form is[46]

$$n(\omega) - 1 = \frac{2}{\pi} \mathscr{P} \int_0^{+\infty} \frac{\omega' k(\omega')}{(\omega')^2 - \omega^2} \, \mathrm{d}\omega'. \tag{5}$$

From the fact that[47]

$$\frac{2}{\pi} \mathscr{P} \int_0^{+\infty} \frac{\omega k(\omega)}{(\omega')^2 - \omega^2} \, \mathrm{d}\omega' = 0, \tag{6}$$

it is possible to remove the pole in Eq. (5). The subtraction of Eq. (6) from Eq. (5) yields

$$n(\omega) - 1 = \frac{2}{\pi} \int_0^{+\infty} \frac{\omega' k(\omega') - \omega k(\omega)}{(\omega')^2 - \omega^2} \, \mathrm{d}\omega', \tag{7}$$

in which the pole is replaced with the apparent singularity. For $\omega' = \omega$, by means of L'Hôpital's rule the integrand in Eq. (7) can be expressed as follows:

$$\lim_{\omega' \to \omega} \frac{\omega' k(\omega') - \omega k(\omega)}{(\omega')^2 - \omega^2} = \frac{k(\omega)}{2\omega} + \frac{1}{2} \frac{\mathrm{d}k}{\mathrm{d}\omega}. \tag{8}$$

In this way the problem of a singularity in the integrand is replaced with the problem of determination of the derivative of the function $k(\omega)$, which will be solved together with the quadrature one. The domain of integration is divided into four regions: (1) from 0 to ω_l, where $k(\omega)$ is calculated with the Drude model; (2) from ω_l to ω_p, where the oscillator model is used; (3) from ω_p to ω_h, where data from Shiles *et al.*[26,27] were employed; and (4) from ω_h to infinity, where the asymptotic expansion of $\epsilon_r(\omega)$ is used to calculate $k(\omega)$. Therefore,

$$n(\omega) - 1 = I_{\mathrm{dm}} + I_{\mathrm{sqm}} + I_{\mathrm{exp}} + I_{\mathrm{ae}}. \tag{9}$$

(The notation exp denotes experimental; other notations are defined below.) Data from Shiles *et al.*[26,27] were used to determine the 256 values of k_i^{exp} between ω_p and ω_h. Coefficients of the cubic spline $C_{i,j}$ are then calculated for k_i^{exp} values. The spline-interpolation curve $k(\omega)$ of the k_i^{exp} function, when given in the form that emphasizes the cubic dependence on ω, is

$$k = k_i^{\mathrm{exp}} + C_{i,1}(\omega - \omega_i) + C_{i,2}(\omega - \omega_i)^2 + C_{i,3}(\omega - \omega_i)^3, \tag{10}$$

where ω is a current variable and ω_i is the value of ω corresponding to the tabulated extinction coefficient value k_i^{exp}. After the spline coefficients have been determined it is easy to obtain the values of the first derivative of $k(\omega)$ in nodes, namely

$$\left. \frac{\mathrm{d}k}{\mathrm{d}\omega} \right|_{\omega = \omega_i} = C_{i,1}, \tag{11}$$

and to evaluate the integrand in I_{exp} with Eq. (7). Other integrals impose fewer problems, although it is impossible to evaluate them analytically. The quadrature is performed by means of the Romberg method with the Carl de Boor algorithm.[48] In I_{dm} the extinction coefficient is given by the Drude model, in I_{sqm} with the semiquantum model, in I_{ae} with the asymptotic expansion of the dielectric constant. The real part of $\epsilon_r(\omega)$ is given by

$$\epsilon_{r1} = 1 - \frac{{\omega_{p,t}}^2}{\omega^2}, \tag{12}$$

where ${\omega_{p,t}}^2 = Ne^2/m\epsilon_0$, and N is a total number density corresponding to the number of 13 electrons/Al atom. ($\omega_{p,t} = 32.86$ eV corresponds to $n_{\mathrm{at}} = 6.028 \times 10^{28}$ at/m^3, where at denotes atom.) The asymptotic expansion for $\epsilon_{r2}(\omega)$ differs from the cubic form:

$$\epsilon_{r2} = \frac{\mathscr{C}}{\omega^{\delta}}, \tag{13}$$

where $\mathscr{C} = 1.42003 \times 10^9$ when ω is in eV, δ is determined by

$$\delta = \begin{cases} 3.97778 + 0.22222 \times 10^{-5}\omega, & \omega < 10^5 \text{ eV} \\ 4.2, & \omega > 10^5 \text{ eV} \end{cases}, \tag{14}$$

and $\mathscr{C}$ and δ were determined when Eq. (13) was fitted to the data in the region from 4 to 10 keV.

In that way the values for refractive index $n(\omega)$ are calculated between ω_p and ω_h. Reflectivity in that region is then obtained from[49]

$$R(\omega) = \frac{[n(\omega) - 1]^2 + k(\omega)^2}{[n(\omega) + 1]^2 + k(\omega)^2}, \tag{15}$$

This equation represents the first approximation for $R(\omega)$ between ω_p and ω_h as combined with the experimental spectrum from ω_l to ω_p and the Drude-model extrapolations from 0 to ω_l, where free-electron behavior was assumed above 10 keV:

$$R^{ae}(\omega) = \frac{{\omega_{p,t}}^4}{16\omega^4} = \left(\frac{16.43}{\omega}\right)^4, \tag{16}$$

where ω is in electron volts. The first approximation for the phase $\theta(\omega)$ of the reflection coefficient $R(\omega)$ is given by the Jahoda–Velický dispersion relation,[46,50]

$$\theta(\omega) = \frac{\omega}{\pi}\int_0^{+\infty} \frac{\log R(\omega') - \log R(\omega)}{(\omega^2 - \omega'^2)}\, d\omega'. \tag{17}$$

The domain of integration is divided into three regions. The quadrature of the second integral is performed in the same way as that for the experimental $k(\omega)$. The values of the integrand have been determined in 404 nodes $\times$ 404 nodes, while the integrand values in singularities ($\omega' = \omega$) were determined through

$$\lim_{\omega' \to \omega} \frac{\log R(\omega') - \log R(\omega)}{(\omega^2 - \omega'^2)} = \frac{-1}{2\omega R(\omega)} \frac{dR}{d\omega}, \tag{18}$$

where the first coefficient of the cubic spline was used as the value of $dR/d\omega$ in the node. After the integrand values had been determined at all frequencies, determination of the spline coefficients for the corresponding values of the integrand for every ω' were performed for each of the 404 values of ω, and this procedure was followed by integration of the spline-interpolation curve from ω_l to ω_h. Therewith the values of the second integral $\theta^{(2)}$ in Eq. (17) were determined in the aforementioned range from $\omega_l = 6.2$ meV to $\omega_h = 10$ keV.

The quadrature of the first $[\theta^{(1)}]$ and the third $[\theta^{(3)}]$ integrals is performed by means of the Romberg method with the Carl de Boor algorithm at the same 404 frequencies as integral $\theta^{(2)}$. Final values for $\theta(\omega)$ obtained in the iterative procedure are presented in Fig. 3. The refractive index, extinction coefficient, and dielectric function were determined at the same 404 points with relations[46]

$$n(\omega) = \frac{1 - R(\omega)}{1 + R(\omega) - 2\sqrt{R(\omega)}\cos[\theta(\omega)]}, \tag{19}$$

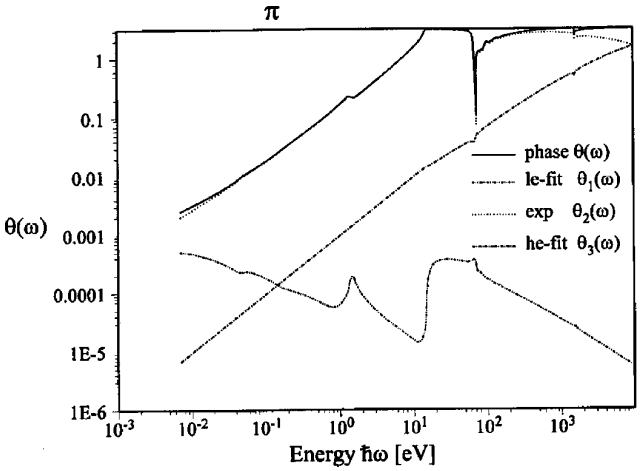

Fig. 3. Phase $\theta(\omega)$ of the reflectivity of aluminum film as derived from the KK analysis in this study: le, low energy; exp, experimental; he, high energy.

$$k(\omega) = \frac{2\sqrt{R(\omega)}\sin[\theta(\omega)]}{1 + R(\omega) - 2\sqrt{R(\omega)}\cos[\theta(\omega)]}, \tag{20}$$

$$\epsilon_{r1}(\omega) = n(\omega)^2 - k(\omega)^2, \tag{21}$$

$$\epsilon_{r2}(\omega) = 2n(\omega)k(\omega). \tag{22}$$

From this stage the procedure returns to the beginning. The new values of the refractive index are combined with experimental values of the extinction coefficient to evaluate the new reflection coefficient from ω_p to ω_h. These values are combined with experimental values for $R(\omega)$ from ω_l to ω_p and then the KK analysis is used to provide new values for the phase from ω_l to ω_h.

It has been proved that this approximation for $n(\omega)$ is better than the previous one obtained directly from the inversion of $k(\omega)$, because of the fact that, in this way, besides experimental values for $k(\omega)$ from ω_p to ω_h, the experimental reflectance spectrum is used from ω_l to ω_p to obtain the refractive index in the region from ω_p to ω_h. After each iteration, the analytical formulas are fitted for high- and low-energy wing extrapolation again to improve the fit. Thus a self-consistent set of optical functions in a wide spectral range from $\omega_l = 6.2$ meV to $\omega_h = 10$ keV is obtained.

4. Results and Sum-Rule Tests

A. Results

Figures 1 and 4 show the final result for $R(\omega)$. Figure 1 compares relevant experimental values with my values obtained with the KK procedure in the region below the plasma frequency. Data from Shiles *et al.*[26,27] are also provided for comparison.

Figure 3 shows the phase $\theta(\omega)$. Values for $\theta(\omega)$ are given by the solid curve, whereas the dashed curves represent integrals in the low-energy region, the high-energy region, and the integral in the region in which experimental data were available.

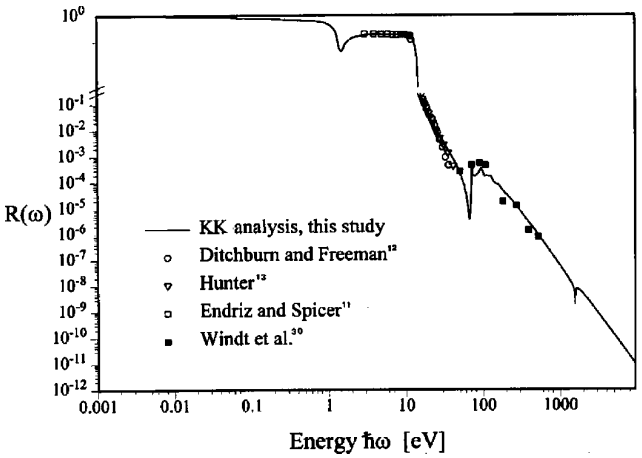

Fig. 4. $R(\omega)$ of a smooth Al film as calculated from optical constants obtained from the KK analysis plus selected experimental data points.

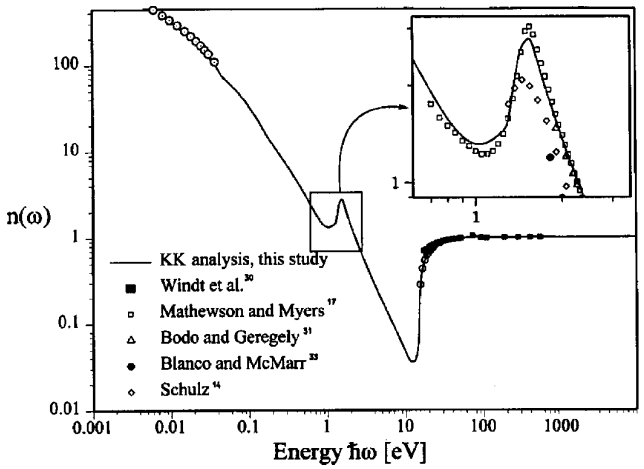

Fig. 6. Plot of the intrinsic refractive index $n(\omega)$ of aluminum film as derived from the KK analysis in this study plus selected experimental data points.

tained from the KK inversion of the reflectance and absorption data. The interband transition at approximately 1.5 eV is noticeable as a peak superimposed on the free-electron absorption. The fine structure noticeable at approximately 72.72 eV is attributable to the *L*-shell absorption, and the absorption edge at approximately 1557 eV to the *K*-shell absorption.

The comparison with experimental values below the plasma frequency where reflectance was used as a starting function in the KK procedure [and the results are independent of the experimental $k(\omega)$] shows the excellent agreement between the experimental and calculated spectra. Data for the ultrahigh-vacuum *in situ* ellipsometric measurements by Mathewson and Myers,[17] the corrected *ex situ* values from Bodo and Gergely,[31] and the measurements by Blanco and McMarr[33] are shown in Fig. 5. Above the plasma frequency the measurements of Windt *et al.*[30] differ significantly from my values and show a stronger absorption for almost 1 order of magnitude, which is probably due to surface roughness. Between the *L*-shell absorption edge and 500 eV, the values of Windt *et al.*[30] are still lower than those obtained by Shiles *et al.*[26,27] by reduction of the $k(\omega)$ values of Haensel *et al.*[20] and Gahwiller and Brown.[19] The obvious problem with the data from Windt *et al.*[30] was recognized by Tanuma *et al.*[51] by employing sum-rule tests on the energy-loss function.

The refractive index is shown in Fig. 6, and it emphasizes the interband absorption peak at 1.5 eV, with the data of Mathewson and Myers,[17] Bodo and Gergely,[31] and Blanco and McMarr.[33] Figure 7 shows a plot of $\epsilon_{r1}(\omega)$ and $\epsilon_{r2}(\omega)$. Selected experimental data points of Mathewson and Myers,[17] Ditchburn and Freeman,[12] and Windt *et al.*[30] are shown for comparison. Final values of the intrinsic optical functions $n(\omega)$ and $k(\omega)$ and the reflectance $R(\omega)$ are given in Table 2.

B. Tests with Inertial and *f*-Sum Rules

Several tests were employed to obtain the criteria to use to stop the procedure, including not only the

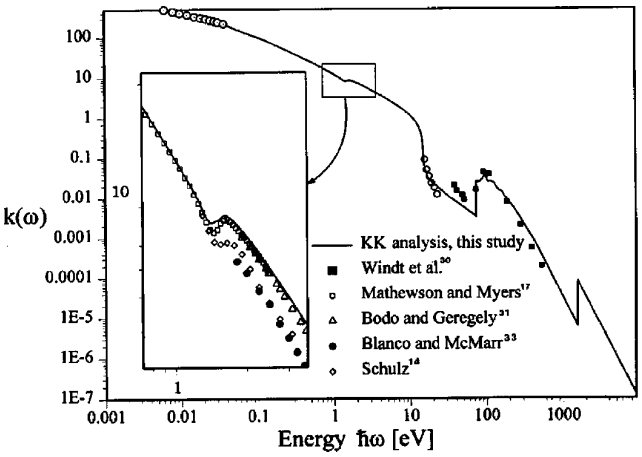

Fig. 5. Plot of the intrinsic extinction coefficient $k(\omega)$ of Al film as derived from the KK analysis in this study plus selected experimental data points.

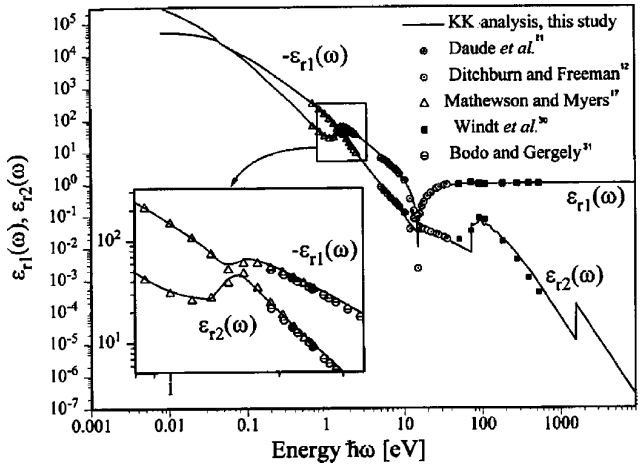

Fig. 7. Plot of the dielectric function of bulk Al film derived from the KK analysis in this study plus selected experimental data points.

Table 2. Values of the Intrinsic Optical Constants $n(\omega)$ and $k(\omega)$ and Reflectance $R(\omega)$ of Aluminum Determined in this Study

$\hbar\omega$ (eV)	λ (μm)	n	k	R
6.1993E−03	2.0000E+02	4.2396E+02	4.8370E+02	9.9591E−01
7.0000E−03	1.7712E+02	3.9793E+02	4.5850E+02	9.9569E−01
8.0590E−03	1.5385E+02	3.6404E+02	4.2962E+02	9.9542E−01
9.0000E−03	1.3776E+02	3.3962E+02	4.0892E+02	9.9520E−01
9.9188E−03	1.2500E+02	3.1881E+02	3.9171E+02	9.9501E−01
1.2399E−02	9.9996E+01	2.7438E+02	3.5435E+02	9.9455E−01
1.5498E−02	8.0001E+01	2.3356E+02	3.2108E+02	9.9409E−01
1.8598E−02	6.6666E+01	2.0263E+02	2.9542E+02	9.9370E−01
2.1697E−2	5.7144E+01	1.7793E+02	2.7534E+02	9.9340E−01
2.4797E−02	5.0000E+01	1.5730E+02	2.5826E+02	9.9314E−01
2.7897E−02	4.4444E+01	1.4005E+02	2.4343E+02	9.9292E−01
3.0996E−02	4.0000E+01	1.2514E+02	2.3019E+02	9.9274E−01
3.7196E−02	3.3333E+01	1.0210E+02	2.0810E+02	9.9243E−01
4.0000E−2	3.0996E+01	9.1955E+01	1.9999E+02	9.9244E−01
4.5000E−02	2.7552E+01	7.5748E+01	1.8178E+02	9.9222E−01
5.0000E−02	2.4797E+01	6.8535E+01	1.6481E+02	9.9143E−01
5.5000E−02	2.2543E+01	6.3554E+01	1.5345E+02	9.9083E−01
6.0000E−02	2.0664E+01	5.8580E+01	1.4423E+02	9.9038E−01
6.5000E−02	1.9075E+01	5.4413E+01	1.3609E+02	9.8992E−01
7.0000E−02	1.7712E+01	5.0951E+01	1.2949E+02	9.8953E−01
8.0000E−02	1.5498E+01	4.3775E+01	1.1839E+02	9.8907E−01
9.0000E−02	1.3776E+01	3.8461E+01	1.0896E+02	9.8854E−01
1.0000E−01	1.2399E+01	3.3519E+01	1.0128E+02	9.8829E−01
1.2000E−01	1.0332E+01	2.6216E+01	8.8197E+01	9.8769E−01
1.4000E−01	8.8561E+00	2.0837E+01	7.8274E+01	9.8738E−01
1.6000E−01	7.7491E+00	1.6755E+01	6.9857E+01	9.8710E−01
1.8000E−01	6.8881E+00	1.4088E+01	6.2841E+01	9.8651E−01
2.0000E−01	6.1993E+00	1.2195E+01	5.7156E+01	9.8582E−01
2.2000E−01	5.6357E+00	1.0742E+01	5.2518E+01	9.8516E−01
2.4000E−01	5.1660E+00	9.5580E+00	4.8593E+01	9.8454E−01
2.6000E−01	4.7687E+00	8.5881E+00	4.5257E+01	9.8395E−01
2.8000E−01	4.4280E+00	7.7757E+00	4.2367E+01	9.8339E−01
3.0000E−01	4.1328E+00	7.0796E+00	3.9826E+01	9.8285E−01
3.2000E−01	3.8745E+00	6.4808E+00	3.7595E+01	9.8236E−01
3.4000E−01	3.6466E+00	5.9564E+00	3.5608E+01	9.8190E−01
3.6000E−01	3.4440E+00	5.4903E+00	3.3814E+01	9.8148E−01
3.8000E−01	3.2628E+00	5.0735E+00	3.2183E+01	9.8108E−01
4.0000E−01	3.0996E+00	4.7097E+00	3.0737E+01	9.8072E−01
4.5000E−01	2.7552E+00	3.9380E+00	2.7580E+01	9.7993E−01
5.0000E−01	2.4797E+00	3.3372E+00	2.5004E+01	9.7927E−01
6.0000E−01	2.0664E+00	2.4738E+00	2.0982E+01	9.7812E−01
7.0000E−01	1.7712E+00	1.9205E+00	1.7991E+01	9.7687E−01
8.0000E−01	1.5498E+00	1.5782E+00	1.5656E+01	9.7493E−01
9.0000E−01	1.3776E+00	1.3899E+00	1.3784E+01	9.7159E−01
1.0000E+00	1.2399E+00	1.3157E+00	1.2245E+01	9.6611E−01
1.1000E+00	1.1271E+00	1.3281E+00	1.0969E+01	9.5775E−01
1.2000E+00	1.0332E+00	1.3998E+00	9.8914E+00	9.4595E−01
1.2400E+00	9.9988E−01	1.4359E+00	9.4939E+00	9.4022E−01
1.2800E+00	9.6863E−01	1.4867E+00	9.0655E+00	9.3270E−01
1.3200E+00	9.3928E−01	1.6784E+00	8.5970E+00	9.1720E−01
1.3600E+00	9.1166E−01	1.9739E+00	8.3058E+00	8.9855E−01
1.4000E+00	8.8561E−01	2.2802E+00	8.1134E+00	8.8091E−01
1.4800E+00	8.3774E−01	2.6945E+00	8.1878E+00	8.6643E−01
1.5200E+00	8.1569E−01	2.7668E+00	8.2573E+00	8.6565E−01
1.5600E+00	7.9478E−01	2.7675E+00	8.3866E+00	8.6904E−01
1.6000E+00	7.7491E−01	2.6154E+00	8.4914E+00	8.7718E−01
1.7000E+00	7.2932E−01	2.1606E+00	8.3565E+00	8.9172E−01
1.8000E+00	6.8881E−01	1.8301E+00	8.0601E+00	8.9969E−01
1.9000E+00	6.5225E−01	1.5724E+00	7.7354E+00	9.0536E−01
2.0000E+00	6.1993E−01	1.3660E+00	7.4052E+00	9.0959E−01
2.2000E+00	5.6357E−01	1.0728E+00	6.7839E+00	9.1472E−01
2.4000E+00	5.1660E−01	8.7340E−01	6.2418E+00	9.1774E−01

Table 2. (**continued**)

$\hbar\omega$ (eV)	λ (μm)	n	k	R
2.6000E+00	4.7687E−01	7.2780E−01	5.7781E+00	9.1996E−01
2.8000E+00	4.4280E−01	6.0790E−01	5.3676E+00	9.2255E−01
3.0000E+00	4.1328E−01	5.2135E−01	5.0008E+00	9.2367E−01
3.4000E+00	3.6466E−01	3.9877E−01	4.3957E+00	9.2504E−01
3.8000E+00	3.2628E−01	3.1474E−01	3.9165E+00	9.2623E−01
4.0000E+00	3.0996E−01	2.8003E−01	3.7081E+00	9.2721E−01
5.0000E+00	2.4797E−01	1.8137E−01	2.9029E+00	9.2614E−01
6.0000E+00	2.0664E−01	1.2677E−01	2.3563E+00	9.2567E−01
7.0000E+00	1.7712E−01	9.4236E−02	1.9519E+00	9.2472E−01
8.0000E+00	1.5498E−01	7.2505E−02	1.6366E+00	9.2425E−01
9.0000E+00	1.3776E−01	5.7167E−02	1.3775E+00	9.2416E−01
1.0000E+00	1.2399E−01	4.6304E−02	1.1555E+00	9.2378E−01
1.1000E+01	1.1271E−01	3.8468E−02	9.5677E−01	9.2283E−01
1.2000E+01	1.0332E−01	3.5753E−02	7.7163E−01	9.1427E−01
1.3000E+01	9.5373E−02	3.6437E−02	5.9086E−01	8.9760E−01
1.4000E+01	8.8561E−02	4.4168E−02	3.9115E−01	8.5790E−01
1.4400E+01	8.6101E−02	5.4863E−02	2.9293E−01	8.1690E−01
1.4600E+01	8.4921E−02	6.7041E−02	2.3420E−01	7.7530E−01
1.4800E+01	8.3774E−02	9.4517E−02	1.6589E−01	6.9150E−01
1.5000E+01	8.2657E−02	1.5065E−01	1.1041E−01	5.4901E−01
1.5100E+01	8.2109E−02	1.7943E−01	9.4223E−02	4.8732E−01
1.5200E+01	8.1569E−02	2.0569E−01	7.9959E−02	4.3649E−01
1.5300E+01	8.1036E−02	2.3344E−01	6.8348E−02	3.8811E−01
1.5400E+01	8.0510E−02	2.5936E−01	6.1407E−02	3.4742E−01
1.5500E+01	7.9990E−02	2.8271E−01	5.6697E−02	3.1404E−01
1.5600E+01	7.9478E−02	3.0373E−01	5.3349E−02	2.8642E−01
1.5800E+01	7.8472E−02	3.4031E−01	4.8320E−02	2.4324E−01
1.6000E+01	7.7491E−02	3.7197E−01	4.4202E−02	2.1036E−01
1.7000E+01	7.2932E−02	4.9131E−01	3.2409E−02	1.1677E−01
1.8000E+01	6.8881E−02	5.7251E−01	2.7681E−02	7.4192E−02
1.9000E+01	6.5255E−02	6.3242E−01	2.4770E−02	5.0923E−02
2.0000E+01	6.1993E−02	6.7912E−01	2.2340E−02	3.6690E−02
2.5000E+01	4.9594E−02	8.1512E−01	1.5894E−02	1.0450E−02
3.0000E+01	4.1328E−02	8.8013E−01	1.1651E−02	4.1028E−03
3.5000E+01	3.5424E−02	9.1802E−01	9.3121E−03	1.8505E−03
4.0000E+01	3.0996E−02	9.4189E−01	7.8466E−03	9.1178E−04
4.5000E+01	2.7552E−02	9.5834E−01	6.6191E−03	4.6407E−04
5.0000E+01	2.4797E−02	9.7048E−01	5.7469E−03	2.3292E−04
5.5000E+01	2.2543E−02	9.7998E−01	5.0004E−03	1.0858E−04
6.0000E+01	2.0664E−02	9.8827E−01	4.3696E−03	3.9652E−05
6.2000E+01	1.9998E−02	9.9143E−01	4.2397E−03	2.3042E−05
6.4000E+01	1.9373E−02	9.9457E−01	4.1092E−03	1.1656E−05
6.6000E+01	1.8786E−02	9.9791E−01	3.8926E−03	4.8906E−06
6.8000E+01	1.8233E−02	1.0019E+00	3.6730E−03	4.2213E−06
7.0000E+01	1.7712E−02	1.0070E+00	3.5425E−03	1.5144E−05
7.1000E+01	1.7463E−02	1.0108E+00	3.4957E−03	3.1665E−05
7.2000E+01	1.7220E−02	1.0169E+00	3.5249E−03	7.3277E−05
7.2050E+01	1.7208E−02	1.0174E+00	3.5108E−03	7.7344E−05
7.2100E+01	1.7196E−02	1.0179E+00	3.4877E−03	8.1982E−05
7.2200E+01	1.7172E−02	1.0192E+00	3.4767E−03	9.2993E−05
7.2300E+01	1.7149E−02	1.0206E+00	3.4400E−03	1.0650E−04
7.2400E+01	1.7125E−02	1.0226E+00	3.4141E−03	1.2783E−04
7.2500E+01	1.7101E−02	1.0249E+00	3.6218E−03	1.5404E−04
7.2600E+01	1.7078E−02	1.0305E+00	4.1164E−03	2.3015E−04
7.2700E+01	1.7054E−02	1.0349E+00	1.2476E−02	3.3231E−04
7.2800E+01	1.7031E−02	1.0305E+00	2.0072E−02	3.2295E−04
7.2900E+01	1.7008E−02	1.0255E+00	2.0012E−02	2.5594E−04
7.3000E+01	1.6984E−02	1.0246E+00	1.9145E−02	2.3706E−04
7.3100E+01	1.6961E−02	1.0262E+00	1.9564E−02	2.6074E−04
7.3200E+01	1.6938E−02	1.0259E+00	2.4227E−02	3.0624E−04
7.3300E+01	1.6915E−02	1.0219E+00	2.6018E−02	2.8319E−04
7.3400E+01	1.6892E−02	1.0194E+00	2.5432E−02	2.5042E−04
7.3500E+01	1.6869E−02	1.0181E+00	2.4831E−02	2.3201E−04
7.3600E+01	1.6846E−02	1.0173E+00	2.4499E−02	2.2130E−04

Table 2. (**continued**)

$\hbar\omega$ (eV)	λ (μm)	n	k	R
7.3700E+01	1.6823E−02	1.0167E+00	2.4375E−02	2.1457E−04
7.3800E+01	1.6800E−02	1.0161E+00	2.4282E−02	2.0882E−04
7.3900E+01	1.6777E−02	1.0156E+00	2.4228E−02	2.0430E−04
7.4000E+01	1.6755E−02	1.0151E+00	2.4184E−02	2.0047E−04
7.4500E+01	1.6642E−02	1.0132E+00	2.4343E−02	1.8926E−04
7.5000E+01	1.6531E−02	1.0118E+00	2.4020E−02	1.7684E−04
7.5500E+01	1.6422E−02	1.0110E+00	2.3955E−02	1.7176E−04
7.6000E+01	1.6314E−02	1.0106E+00	2.3853E−02	1.6857E−04
7.7000E+01	1.6102E−02	1.0095E+00	2.5180E−02	1.7931E−04
7.8000E+01	1.5896E−02	1.0078E+00	2.4757E−02	1.6727E−04
7.9000E+01	1.5694E−02	1.0075E+00	2.4501E−02	1.6302E−04
8.0000E+01	1.5498E−02	1.0075E+00	2.4476E−02	1.6253E−04
8.2000E+01	1.5120E−02	1.0077E+00	2.5460E−02	1.7536E−04
8.4000E+01	1.4760E−02	1.0074E+00	2.6826E−02	1.9208E−04
8.6000E+01	1.4417E−02	1.0065E+00	2.8232E−02	2.0852E−04
8.8000E+01	1.4089E−02	1.0060E+00	2.8956E−02	2.1739E−04
9.0000E+01	1.3776E−02	1.0058E+00	3.0918E−02	2.4595E−04
9.2000E+01	1.3477E−02	1.0041E+00	3.3392E−02	2.8181E−04
9.4000E+01	1.3190E−02	1.0012E+00	3.5311E−02	3.1159E−04
9.6000E+01	1.2915E−02	9.9652E−01	3.5883E−02	3.2595E−04
9.8000E+01	1.2652E−02	9.9265E−01	3.3061E−02	2.8881E−04
1.0000E+02	1.2399E−02	9.9123E−01	2.9920E−02	2.4509E−04
1.0500E+02	1.1808E−02	9.9285E−01	2.4415E−02	1.6293E−04
1.1000E+02	1.1271E−02	9.9415E−01	2.5452E−02	1.7148E−04
1.1500E+02	1.0781E−02	9.9233E−01	2.4928E−02	1.7136E−04
1.2000E+02	1.0332E−02	9.9139E−01	2.4063E−02	1.6467E−04
1.2500E+02	9.9188E−03	9.8941E−01	2.3421E−02	1.6689E−04
1.3000E+02	9.5373E−03	9.8761E−01	2.0606E−02	1.4633E−04
1.3500E+02	9.1841E−03	9.8793E−01	1.7765E−02	1.1674E−04
1.4000E+02	8.8561E−03	9.8883E−01	1.6304E−02	9.8733E−05
1.4500E+02	8.5507E−03	9.8934E−01	1.5437E−02	8.8925E−05
1.5000E+02	8.2657E−03	9.8966E−01	1.4773E−02	8.2117E−05
1.6000E+02	7.7491E−03	9.8912E−01	1.3728E−02	7.7554E−05
1.7000E+02	7.2932E−03	9.8909E−01	1.0987E−02	6.0609E−05
1.8000E+02	6.8881E−03	9.9007E−01	9.6517E−03	4.8404E−05
1.9000E+02	6.5255E−03	9.9054E−01	8.4716E−03	4.0688E−05
2.0000E+02	6.1993E−03	9.9111E−01	7.5099E−03	3.4179E−05
2.5000E+02	4.9594E−03	9.9313E−01	4.1863E−03	1.6300E−05
3.0000E+02	4.1328E−03	9.9480E−01	2.3492E−03	8.1735E−06
4.0000E+02	3.0996E−03	9.9694E−01	9.6887E−04	2.5787E−06
5.0000E+02	2.4797E−03	9.9797E−01	4.3503E−04	1.0809E−06
6.0000E+02	2.0664E−03	9.9860E−01	2.2001E−04	4.9938E−07
7.0000E+02	1.7712E−03	9.9898E−01	1.1811E−04	2.6130E−07
8.0000E+02	1.5498E−03	9.9924E−01	7.2992E−05	1.4699E−07
9.0000E+02	1.3776E−03	9.9940E−01	4.6771E−05	8.9319E−08
1.0000E+03	1.2399E−03	9.9953E−01	3.1115E−05	5.6611E−08
1.1000E+03	1.1271E−03	9.9961E−05	2.1586E−05	3.7224E−08
1.2000E+03	1.0332E−03	9.9968E−01	1.5628E−05	2.5095E−08
1.3000E+03	9.5373E−04	9.9974E−01	1.1636E−05	1.7125E−08
1.4000E+03	8.8561E−04	9.9979E−01	8.9400E−06	1.1529E−08
1.4500E−03	8.5507E−04	9.9981E−01	7.8422E−06	9.2016E−09
1.5000E+03	8.2657E−04	9.9983E−01	6.8049E−06	6.8662E−09
1.5200E−03	8.1569E−04	9.9985E−01	6.4818E−06	5.7605E−09
1.5400E+03	8.0510E−04	9.9987E−01	6.1901E−06	4.2509E−09
1.5500E+03	7.9990E−04	9.9989E−01	6.0484E−06	2.7904E−09
1.5520E+03	7.9887E−04	9.9991E−01	1.1026E−05	2.2573E−09
1.5540E+03	7.9785E−04	9.9991E−01	2.3687E−05	2.0392E−09
1.5580E+03	7.9580E−04	9.9992E−01	3.2911E−05	1.8775E−09
1.5590E+03	7.9529E−04	9.9992E−01	4.1131E−05	1.8451E−09
1.5600E+03	7.9478E−04	9.9993E−01	4.9998E−05	1.9542E−09
1.5620E−03	7.9376E−04	9.9992E−01	7.1847E−05	2.7496E−09
1.5640E+03	7.9274E−04	9.9990E−01	8.5418E−05	4.1195E−09
1.5800E+03	7.8472E−04	9.9987E−01	7.8480E−05	6.0380E−09

Table 2. (continued)

$\hbar\omega$ (eV)	λ (μm)	n	k	R
1.5950E+03	7.7734E−04	9.9986E−01	7.4862E−05	6.6327E−09
1.6750E+03	7.4021E−04	9.9984E−01	6.1633E−05	7.1236E−09
1.7000E+03	7.2932E−04	9.9984E−01	5.7974E−05	6.9756E−09
1.8000E+03	6.8881E−04	9.9985E−01	4.7138E−05	6.1191E−09
1.9000E+03	6.5255E−04	9.9986E−01	3.8497E−05	5.2251E−09
2.0000E+03	6.1993E−04	9.9987E−01	3.2079E−05	4.4083E−09
2.5000E+03	4.9594E−04	9.9991E−01	1.3642E−05	1.9442E−09
3.0000E+03	4.1328E−04	9.9994E−01	7.1408E−06	9.4114E−10
3.5000E+03	3.5424E−04	9.9995E−01	4.0484E−06	5.1163E−10
4.0000E+03	3.0996E−04	9.9997E−01	2.4843E−06	2.9845E−10
5.0000E+03	2.4797E−04	9.9998E−01	1.0726E−06	1.2137E−10
6.0000E+03	2.0664E−04	9.99984E−01	5.5102E−07	5.7915E−11
7.0000E+03	1.7712E−04	9.99989E−01	3.1463E−07	3.1072E−11
8.0000E+03	1.5498E−04	9.99991E−01	1.9173E−07	1.8104E−11
9.0000E+03	1.3776E−04	9.99993E−01	1.2488E−07	1.1245E−11
9.5000E+03	1.3051E−04	9.99994E−01	1.2720E−07	9.0423E−12
1.0000E+04	1.2399E−04	9.999946E−01	8.2410E−08	7.5642E−12

usual test of the difference between functions obtained in two succeeding iterations but also two groups of tests with the sum rules.[52,53]

1. *Inertial Sum Rules*

Inertial sum rules are connected with the behavior of the real part of the refractive index and the dielectric constant. The sum rule for $n(\omega)$ that states that the average value of the refractive index is unity[54] is usually normalized by the introduction of the verification parameter ζ in the following manner[52]:

$$\zeta = \frac{\int_0^{+\infty} [n(\omega) - 1]\mathrm{d}\omega}{\int_0^{+\infty} |n(\omega) - 1|\mathrm{d}\omega}. \tag{23}$$

The Drude model with the frequency-dependent damping constant is used for low-frequency extrapolation. Parameters used in this calculation are presented in Table 3. For high-frequency extrapolation the asymptotic expansion for $n(\omega)$ is employed:

$$n(\omega) = 1 - \frac{{\omega_{p,t}}^2}{2\omega^2}, \tag{24}$$

where $\omega_{p,t} = 32.86$ eV corresponds to 13 electrons/Al atom. With our $n(\omega)$ values, $\zeta = 2 \times 10^{-4}$ is obtained, which is completely satisfactory. The calculation of parameter ζ, which was performed by Altarelli and Smith[52] on data from Sasaki and Inokuti, gives $\zeta = 0.17$, which indicates the large inconsistency in the $k(\omega)$ values. The value of $\zeta = 0.06$ is obtained[52] when the data of Bennett and Bennett[22] were employed instead of the data used by Sasaki and Inokuti in the IR. The best value obtained hitherto[26] is $\zeta = -2 \times 10^{-3}$, 1 order of magnitude higher than my value $\zeta = 2 \times 10^{-4}$.

Table 3. Drude-Model Parameter Values Employed for the Low-Frequency-Region Extrapolations

Ω_p (eV)	Γ (meV)	τ (s)
11.6	53.3	7.75×10^{-16}
11.3	49.9	0

This test casts light on that part of the spectrum (the IR) for which *f*-sum rules are not sensitive. All forms of *f*-sum rules contain the factor $\omega k(\omega)$ in the integrand, which causes insufficient sensitivity below 0.1 eV, as noticed by Altarelli and Smith[52] in their analysis.

The second rule employed here is an inertial rule for ϵ_{r1} (the dc-conductivity sum rule)[52]:

$$\int_0^{+\infty} [\epsilon_{r1}(\omega) - 1]\mathrm{d}\omega = \frac{-\pi}{2\epsilon_0}\sigma_0. \tag{25}$$

Because it is sensitive only to the free-electron part of the spectrum,[55] this integral provides a good test of intraband-dispersion functions and free-electron ex-

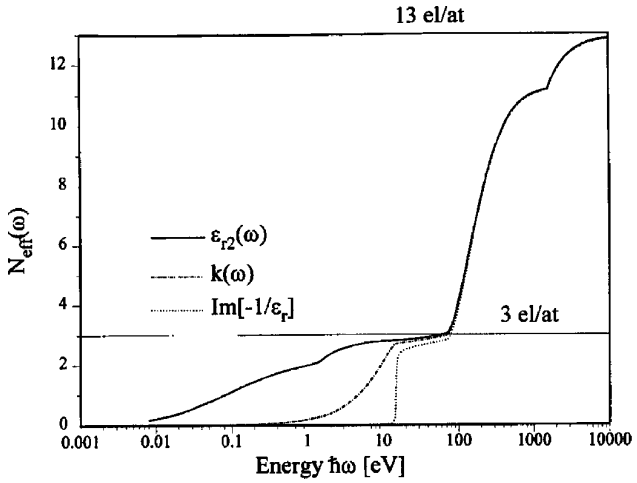

Fig. 8. Number density of electrons/Al atom $N_{\mathrm{eff}}(\omega)$ that contribute to absorption processes, as obtained by means of the finite-energy *f*-sum rules: el, electrons; at, atom.

trapolations. The quadrature is performed with the Drude-model extrapolation to zero, the asymptotic expansion in the high-frequency region, and integration of the cubic-spline-interpolation function between $\omega_l = 6.2$ meV and $\omega_h = 10$ keV. This process yields $\sigma_0 = 3.44 \times 10^7\ 1/\Omega\text{m}$ ($\rho_0 = 2.90\ \mu\Omega\text{cm}$), which is in good agreement with the electrical-conductivity data for bulk Al samples $\sigma_0 = 3.5(3) \times 10^7\ 1/\Omega\text{m}$, ($\rho_0 = 2.8(3)\ \mu\Omega\text{cm}$), which were obtained from Table F-142 in Ref. 56 for Al wire.

2. *f-Sum Rules*

The second group of tests is performed by means of the finite-energy *f*-rules,[53,55] which define the number density of electrons contributing to the absorption processes. These rules enable one to test dissipative functions such as the imaginary part of the complex dielectric constant ϵ_{r2}, the extinction coefficient k, and the electron-energy-loss function $\text{Im}(-1/\epsilon_r)$:

$$N_{\text{eff}|\epsilon_r} = \frac{2m\epsilon_0}{\pi e^2} \int_0^{\omega} \omega' \epsilon_{r2}(\omega')\,\mathrm{d}\omega', \tag{26}$$

$$N_{\text{eff}|k} = \frac{4m\epsilon_0}{\pi e^2} \int_0^{\omega} \omega' k(\omega')\,\mathrm{d}\omega', \tag{27}$$

$$N_{\text{eff}|\epsilon_r^{-1}} = -\frac{2m\epsilon_0}{\pi e^2} \int_0^{\omega} \omega'\ \text{Im}\left[\epsilon_r^{-1}(\omega')\right]\mathrm{d}\omega'. \tag{28}$$

Indices ϵ_r, k, and ϵ_r^{-1} denote the effective number density obtained from partial-sum rules connected with the related function. It is evident that these integrals are not equivalent in the sense of the determination of the $N_{\text{eff}}(\omega)$. However, for sufficiently large frequencies, all the electrons are excited, so that all the integrals saturate at 13 electrons/Al atom. It is easy to understand the differences between $N_{\text{eff}}(\omega)$ as defined by Eqs. (26)–(28) if one keeps in mind that $\epsilon_{r2}(\omega)$ describes the dissipation of energy from the electromagnetic wave, that $k(\omega)$ describes the attenuation of wave magnitude, and that $\text{Im}[\epsilon_r^{-1}(\omega)]$ is connected with the loss of energy of the electrons passing through the film.

Figure 8 presents the results for $N_{\text{eff}}(\omega)$ evaluated in this study. The Drude model is used for low-energy extrapolation and the asymptotic expansion of $\epsilon_r(\omega)$ for the high-energy region.

Evaluation of all these integrals yields $N = 13$ electrons/Al atom, which provides an additional confirmation of the correctness of the numerical procedure itself and of the good choice of experimental data. Thus, the first group of tests enabled me to test the validity of the dispersion functions, and the second group provided the test for dissipative functions. These tests are far more relevant than the simple numerical-procedure convergency test because they not only test the accuracy of the numerical algorithm, but also demonstrate the correct extrapolations and the internal consistency of the experimental data. In addition, they prove that the obtained functions are really *intrinsic* optical functions of aluminum.

5. Conclusion

The results obtained in such a procedure exceed those of the classical KK inversion for several reasons. The advantage of this iterative method compared with the usual KK procedure stems first from the fact that the procedure does not depend on the specific model of the optical constants, and second, and primarily, from the iteration of the extinction-coefficient inversion and reflectance inversion.

The model is used only to provide the initial values of the optical constants, which are then improved in the succeeding stages of the iterative process by means of the experimental values of the extinction coefficient and reflectance. The alternative inversion of $k(\omega)$ and $R(\omega)$ leads to the successive improvement of the optical constants in the first (ω_l to ω_p) and second (ω_p to ω_h) parts of the spectrum.

The number of iterations needed can be significantly reduced by a good model approximation, which leads consequently to a reduction in computational errors accumulated in the numerical procedure. In this study, values of the semiquantum-model parameters were carefully chosen to provide optical constants that are in close agreement with both the experiment and the theory. In the last stage of the procedure only two complete iterations were needed to obtain the final values of the optical constants.

References

1. W. A. Harrison, "Electronic structure and the properties of metals. II. Application to zinc," Phys. Rev. **129,** 2512–2524 (1963).
2. W. A. Harrison, "Parallel-band effects in interband optical absorption," Phys. Rev. **147,** 467–469 (1966).
3. N. W. Ashcroft and K. Sturm, "Interband absorption and the optical properties of polyvalent metals," Phys. Rev. B **3,** 1898–1910 (1971).
4. S. P. Singhal and J. Callaway, "Self-consistent energy bands in aluminum—improved calculation," Phys. Rev. B **16,** 1744–1746 (1977).
5. J. A. Nelson and P. J. Bunyan, "Calculation of bandstructure of aluminum using the model potential method, J. Phys. F **7,** 1467–1475 (1977).
6. F. Szmulowicz and B. Segall, "Calculation of optical spectra of aluminum," Phys. Rev. B **24,** 892–903 (1981).
7. E. G. Maksimov, I. I. Mazin, S. N. Rashkeev, and Y. A. Uspenski, "First principles calculations of the optical properties of metals," J. Phys. F **18,** 833–849 (1988).
8. K.-H. Lee and K. J. Chang, "First-principles study of the optical properties and the dielectric response of Al," Phys. Rev. B **49,** 2362–2367 (1994).
9. H. E. Bennett, M. Silver, and E. J. Ashley, "Infrared reflectance of aluminum in ultrahigh vacuum," J. Opt. Soc. Am. **53,** 1089–1095 (1963).
10. G. Hass and J. E. Waylonis, "Optical constants and reflectance and transmittance of evaporated aluminum in the visible and ultraviolet," J. Opt. Soc. Am. **51,** 719–722 (1961).
11. J. G. Endriz and W. E. Spicer, "Study of aluminum films I. Optical studies of reflectance drops and surface oscillations on controlled-roughness films," Phys. Rev. B **4,** 4144–4159 (1971).
12. R. W. Ditchburn and G. H. C. Freeman, "The optical constants

of aluminium from 12 to 36 eV," Proc. R. Soc. London Ser. A **294,** 20–37 (1966).
13. W. R. Hunter, "Optical constants of metals in the extreme ultraviolet. II. Optical constants of aluminum, magnesium, and indium at wavelengths shorter than their critical wavelengths," J. Opt. Soc. Am. **54,** 208–212 (1964).
14. L. G. Schulz, "The optical constants of silver, gold, copper, and aluminum. I. The absorption coefficient *k*," J. Opt. Soc. Am. **44,** 357–362 (1954).
15. L. G. Schulz and F. R. Tangherlini, "The optical constants of silver, gold, copper, and aluminum. II. The index of refraction *n*," J. Opt. Soc. Am. **44,** 362–368 (1954).
16. D. Beaglehole, "The ultraviolet absorption of the noble metals," in *Optical Properties and Electronic Structure of Metals and Alloys,* F. Abeles, ed. (North-Holland, Amsterdam, 1966), pp. 154–163.
17. A. G. Mathewson and H. P. Myers, "Absolute values of the optical constants of some pure metals," Phys. Scr. **4,** 291–292 (1971).
18. A. Balzarotti, A. Bianconi, and E. Burattini, "Role of the density of conduction states on the L2-3 absorption spectrum of aluminum," Phys. Rev. B **9,** 5003–5007 (1974).
19. C. Gahwiller and F. C. Brown, "Photoabsorption near the LII-III edge of silicon and aluminum," Phys. Rev. B **2,** 1918–1925 (1970).
20. R. Haensel, B. Sontag, C. Kunz, and T. Sasaki, "Contribution of the L shell to the total absorption cross section of aluminum," J. Appl. Phys. **40,** 3046–3047 (1969).
21. A. Daude, M. Priol, and S. Robin, "Propriétés optiques dans l'ultraviolet lointain de couches d'aluminium évaporées en ultravide et non exposées à l'air," C. R. Acad. Sci. Ser. B **263,** 1178–1181 (1966).
22. H. E. Bennett and J. M. Bennett, "Validity of the Drude theory for silver, gold and aluminum in the infrared," in *Optical Properties and Electronic Structure of Metals and Alloys,* F. Abeles, ed. (North-Holland, Amsterdam, 1966), pp. 175–189.
23. H. Ehrenreich, H. R. Philipp, and B. Segall, "Optical properties of aluminum," Phys. Rev. **132,** 1918–1928 (1963).
24. H. R. Philipp and H. Ehrenreich, "Optical constants in the x-ray range," J. Appl. Phys. **35,** 1416–1419 (1964).
25. H. J. Hagemann, W. Gudat, and C. Kunz, "Optical constants from the far infrared to the x-ray region: Mg, Al, Cu, Ag, Au, Bi, C, and Al_2O_3," J. Opt. Soc. Am. **65,** 742–744 (1975).
26. E. Shiles, T. Sasaki, M. Inokuti, and D. Y. Smith, "Self-consistency and sum-rule tests in the Kramers–Kronig analysis of optical data: application to aluminum," Phys. Rev. B **22,** 1612–1628 (1980).
27. D. Y. Smith, E. Shiles, and M. Inokuti, "The optial properties of metallic aluminum," in *Handbook of Optical Constants of Solids,* E. D. Palik, ed. (Academic, Orlando, Fla., 1985), pp. 369–408.
28. J. R. Blanco, K. Vedam, and P. J. McMarr, "Roughness measurements by spectroscopic ellipsometry," Appl. Opt. **24,** 3773–3779 (1985).
29. M. A. Ordal, R. J. Bell, Jr., R. W. Alexander, L. A. Newquist, and M. R. Querry, "Optical properties of Al, Fe, Ti, Ta, W, and Mo at submillimeter wavelengths," Appl. Opt. **27,** 1203–1209 (1988).
30. D. L. Windt, Jr., W. C. Cash, M. Scott, P. Arendt, B. Newnam, R. F. Fisher, A. B. Swartzlander, P. Z. Takacs, and J. M. Pinneo, "Optical constants for thin films of C, diamond, Al, Si, and CVD SiC from 24 Å to 1216 Å," Appl. Opt. **27,** 279–295 (1988).
31. Z. Bodó and G. Gergely, "Intrinsic optical constants of aluminum," Appl. Opt. **26,** 2065–2067 (1987).
32. M. L. Scott, P. N. Arendt, B. J. Cameron, J. M. Saber, and B. E. Newnam, "Extreme ultraviolet reflectance degradation of aluminum and silicon from surface oxidation," Appl. Opt. **27,** 1503–1507 (1988).
33. J. R. Blanco and P. J. McMarr, "Roughness measurements of Si and Al by variable angle spectroscopic ellipsometry," Appl. Opt. **30,** 3210–3220 (1991).
34. H. V. Nguyen, I. An, and R. W. Collins, "Evolution of the optical functions of thin-film aluminum: a real time spectroscopic ellipsometry study," Phys. Rev. B **47,** 3947–3965 (1993).
35. D. C. Jiles and M. P. Staines, "Piezo optic properties of aluminum," Solid State Commun. **47,** 37–41 (1983).
36. D. Y. Smith and B. Segal, "Intraband and interband processes in the infrared spectrum of metallic aluminum," Phys. Rev. B **34,** 5191–5198 (1986).
37. C. J. Powell, "Analysis of optical and inelastic-electron-scattering data. II. Application to Al," J. Opt. Soc. Am. **60,** 78–93 (1970).
38. S. Roberts, "Optical properties of nickel and tungsten and their interpretation according to Drude's formula," Phys. Rev. **114,** 104–115 (1959).
39. H. Ehrenreich and H. R. Philipp, "Optical properties of Ag and Cu," Phys. Rev. **128,** 1622–1629 (1962).
40. K. Sturm and N. W. Ashcroft, "Nonlocal effects in absorption edges: energy-dependent pseudopotentials," Phys. Rev. B **10,** 1343–1349 (1974).
41. M. I. Marković and A. D. Rakić, "Determination of the reflection coefficients of laser light of wavelengths $\lambda \in$ (0.22 μm, 200 μm) from the surface of aluminum using the Lorentz-Drude model," Appl. Opt. **29,** 3479–3483 (1990).
42. R. N. Gurzhi and M. I. Kaganov, "Vliyanie mezhelektronih stolknovenii na opticheskie svoistva metallov" Zh. Eksp. Teor. Fiz. **49,** 941–943, (1965).
43. G. R. Parkins, W. Lawrence, and R. W. Christy, "Intraband optical conductivity $\sigma(\omega, T)$ of Cu, Ag, and Au: contribution from electron–electron scattering," Phys. Rev. B **23,** 6408–6415 (1981).
44. M. I. Marković and A. D. Rakić, "Determination of optical properties of aluminium including electron reradiation in the Lorentz–Drude model," Opt. Laser Technol. **22,** 394–398 (1990).
45. F. Wooten, *Optical Properties of Solids* (Academic, New York, 1972).
46. F. Stern, "Elementary theory of the optical properties of solids," in *Solid State Physics,* F. Steitz and D. Turnbull, eds. (Academic, New York, 1963), Vol. 15, pp. 299–408.
47. F. W. King, "Sum rules for the optical constants," J. Math. Phys. **17,** 1509–1514 (1976).
48. C. de Boor, "CADRE: an algorithm for numerical quadrature," in *Mathematical Software,* J. R. Rice, ed. (Academic, New York, (1971), Chap. 7.
49. M. Born and E. Wolf, *Principles of Optics* (Pergamon, New York, 1959).
50. F. C. Jahoda, "Fundamental absorption of barium oxide from its reflectivity spectrum," Phys. Rev. **107,** 1261–1265, 1957.
51. S. Tanuma, C. J.Powell, and D. R. Penn, "Use of sum rules on the energy-loss function for the evaluation of experimental optical data," J. Electron Spectrosc. Relat. Phenom. **62,** 95–109 (1993).
52. M. Altarelli and D. Y. Smith, "Superconvergence and sum rules for the optical constants: physical meaning, comparison with experiment, and generalization," Phys. Rev. B **9,** 1290–1298 (1974).
53. D. Y. Smith and E. Shiles, "Finite-energy *f*-sum rules for valence electrons," Phys. Rev. B **17,** 4689–4694 (1978).
54. M. Altarelli, D. L. Dexter, H. M. Nussenzveig, and D. Y. Smith, "Superconvergence and sum rules for the optical constants," Phys. Rev. B **6,** 4502–4509 (1972).
55. D. Y. Smith, "Dispersion theory, sum rules, and their application to the analysis of optical data," in *Handbook of Optical Constants of Solids,* E. D. Palik, ed. (Academic, Orlando, Fla., 1985), pp. 35–68.
56. R. C. Weast, ed., *CRC Handbook of Chemistry and Physics* 70th ed. (CRC Press, Boca Raton, Fla., 1990).